ENVIRONMENTAL RESEARCH
LETTERS

LETTER • OPEN ACCESS

Greenspace, bluespace, and their interactive influence on urban thermal environments

To cite this article: Leiqiu Hu and Qi Li 2020 *Environ. Res. Lett.* **15** 034041

Environmental Research Letters

CrossMark

OPEN ACCESS

RECEIVED
21 October 2019

REVISED
13 January 2020

ACCEPTED FOR PUBLICATION
15 January 2020

PUBLISHED
3 March 2020

LETTER

Greenspace, bluespace, and their interactive influence on urban thermal environments

Leiqiu Hu[1,3] and **Qi Li**[2,3]

[1] Department of Atmospheric and Earth Science, The University of Alabama in Huntsville, Huntsville, AL 35805, United States of America
[2] School of Civil & Environmental Engineering, Cornell University. Ithaca, NY 14853, United States of America
[3] L Hu and Q Li contributed equally to this work.

E-mail: leiqiu.hu@uah.edu

Keywords: urban thermal environment, green space, blue space, interactive effect

Supplementary material for this article is available online

Abstract

Urban land use land cover (LULC) change raises ambient temperature and modifies atmospheric moisture, which increases heat-related health risks in cities. Greenspace and bluespace commonly coexist in urban landscapes and are nature-based heat mitigation strategies. Yet, their interactive effects on urban thermal environments are rarely assessed and it remains unclear how extreme heat events (EHEs) affect their ability to regulate human thermal comfort. Using multi-year observations from a dense urban observational network in Madison, WI, we found that green and blue spaces jointly modify the intraurban spatiotemporal variability of temperature and humidity, and the resultant effects on thermal comfort show diurnal and seasonal asymmetry. Greenspace is more effective at cooling throughout the year, particularly at night. Accelerated cooling efficiency is found in areas with dominant greenspace coverage and little co-influence from bluespace. The thermal comfort benefit due to greenspaces can be offset by bluespaces because of intensified nighttime warming and humidifying effects during the warm months, although a weak daytime cooling of bluespace is observed. EHEs enhance bluespace cooling, but the overall joint thermal regulation remains the same due to the enhanced moisture effect. Our findings suggest that diverse outcomes of green and blue spaces cross multiple temporal scales should be holistically assessed in urban planning. The analysis framework based on generalized additive models is robust and transferable to other cities and applications to disentangle the nonlinear co-influences of different drivers of urban environmental phenomena.

1. Introduction

Cities house more than half of the global population, serve as the nexus among energy, climate, and humanity in the Anthropocene, and are one of the most notable forms of land use land cover (LULC) change on the Earth's surface (Steffen *et al* 2018). The pronounced LULC changes in cities lead to elevated urban temperatures compared to rural or suburban areas, and is well known as the urban heat island effect (UHI) (Oke 1995). Climate change enhances the frequency and severity of extreme heat events (Rahmstorf and Coumou 2011, Oleson *et al* 2015), which strongly interact with UHI (Hu *et al* 2015) and lead to a myriad of health and environmental repercussions for urban populations (Guo *et al* 2018). Urban heat-related mortality and morbidity together with other environmental stresses, such as a surge in energy and water demand, have spurred actions to combat heat extremes in cities. One heat mitigation strategy is to use high-albedo roofs and paved roads and/or rooftop high-performance solar cells to alleviate surface heating during the daytime (e.g. (Senevir-atne *et al* 2018)), which requires cautious implementation for the desired outcomes (Kapsalis *et al* 2014, Ma *et al* 2017). Another effective heat abatement strategy is the use of nature-based solutions (Frantzeskaki *et al* 2019), such as restoration of city parks, tree lined streets, gardens, and green facades, i.e. 'greenspace' (Aram *et al* 2019). Greenspace cooling is mainly achieved by evapotranspiration, shading, and reduced heat storage (Oke *et al* 1989, Grimmond 2007, Rahman *et al* 2015). In addition, the local climate can be improved through careful design of urban morphology, such as city ventilation, waste heat dispersion and renewable energy penetration (Oke 1988, Adelia *et al* 2019, He *et al* 2019a).

Meanwhile, throughout the history of humanity, many cities have sprung up along rivers, shorelines and coastal regions (Grimm *et al* 2008). These waterfront urban agglomerations are often densely populated with prosperous economies (Small 2004). 'Bluespace' includes both natural and man-made open water surfaces such as oceans, lakes, wetlands, ponds, canals, and rivers (Gunawardena *et al* 2017). Besides the significant historical, cultural and geopolitical values of watercourses, urban bluespace has been recognized in urban planning and architectural design for its cooling benefits (Santamouris *et al* 2017). However, these benefits remain inconclusive since only a few observational studies show evidence of air temperature reduction and/or warming, mainly either at a small scale or during a short period (Völker *et al* 2013, Gunawardena *et al* 2017). Numerical modeling under idealized conditions and meta-analyses that are primarily concluded from satellite observation-based studies suggest a non-trivial role of bluespace in modulating the temperature, albeit with a diverse range of conclusions (Völker *et al* 2013, Gunawardena *et al* 2017). Two general observations emerge: first, the daytime cooling effects of bluespace range from 0.4 °C −2.0 °C for ambient air temperature and 0.95 °C–5.4 °C for surface temperature, depending on the inherent properties of the bluespace and site-specific climatic factors (Völker *et al* 2013, Gunawardena *et al* 2017); second, as the high thermal inertia of bluespace reduces the diurnal ambient temperature variation, nighttime warming effect has been reported in a few observational (e.g., (Völker *et al* 2013)) and modeling studies (e.g., (Theeuwes *et al* 2013)).

One as yet largely unexplored aspect for urban heat stress mitigation is the interaction between greenspace and bluespace (Gunawardena *et al* 2017). In natural environments, vegetation has been shown to interact synergistically with bluespace, such as lowering the summer air temperature above rivers by providing shading or even reducing evaporative cooling of water bodies because of vegetation's wind sheltering effect (Gunawardena *et al* 2017). The net outcomes of interaction for improving human comfort in urban settings remain unexamined. Their conditional cooling capacity, i.e., how effective green or blue space cools given the presence of the other, is also largely unknown. An assessment solely on urban greenspace may be biased by overlooking the potential interactive effects between green and blue spaces as they commonly coexist in urban areas and blue spaces play a non-negligible role in modulating the thermal environment. With increasing efforts of urban greening (e.g. the 'Million Tree Program' in many mega-cities (Frantzeskaki *et al* 2019)) and low-impact development with water-sensitive urban design (Coutts *et al* 2014, He *et al* 2019b), there is a pressing need to accurately evaluate the programs' effectiveness at the city scale, given the existing green or blue spaces.

The outcomes of heat mitigation strategies may have distinct diurnal and seasonal variability; their cooling capacity can also differ across spatial scales (Ziter *et al* 2019). More importantly, their cooling capacity during extreme temperature events is not well understood due to the complex interactions of radiative, convective, evaporative processes as well as the vegetation's physiological responses to the temperature extremes (Oke *et al* 1989, Rahman *et al* 2015); consequently, the effectness of mitigation strategies during extreme temperature events are difficult to predict (Guo *et al* 2018). The spatial planning of heat mitigation strategies in urban areas therefore requires comprehensive information on multi-scale variability and detailed effectiveness (linear or nonlinear relation to heat abatement) to efficiently achieve the expected outcome without overlooking or introducing unexpected risks under all conditions.

Here, we aim to address two key questions to bridge the important knowledge gaps: (1) How do green and blue spaces jointly influence the intra-urban diurnal and seasonal variation of human thermal comfort? (2) What is their combined thermal regulating performance in the long-term and under extremely hot conditions? We take the interplay of temperature, moisture, and wind speed to measure thermal comfort, using Madison, WI as an example. Multi-year observations of ambient temperature and humidity from a spatially dense urban network are used to quantify the integrative effects of urban green and blue spaces on the urban thermal environment. Moreover, the generalized additive models (GAMs) used in this study are robust and transferable to other applications to disentangle the nonlinear co-influences of different drivers of urban environmental phenomena.

2. Materials and methods

Madison, WI is a typical mid-size US metropolitan region, with a population of roughly 660,000 in 2018 (US Census Bureau/Population Division 2019). The unique city setting as an isthmus between two lakes, Mendota and Monona, significantly influences the spatial distribution of temperature and moisture over the urban core and the suburban areas around the lakes. Around the built area, the dominant land use types include cropland, lakes, and forests. Madison has a humid continental climate, featuring warm summers and cold winters.

2.1. Data and data preparation

The spatially dense meteorological network from the US Long-Term Ecological Research Network (LTER) of North Temperate Lakes over the metropolitan area of Madison, Wisconsin is used for this study (Kucharik 2018). 152 HOBO U23 Pro V2 sensors were attached on streetlight poles at a height of about 3.5 m over various landscapes (Schatz and Kucharik 2014). The network provides the half-hourly record of the ambient temperature (T_a [°C]) and relative humidity (*RH* [%]) from March 2012 to December 2017. We conducted the initial quality check by comparing the network observations with the hourly weather-station observations from the Data County Regional Airport (WBAN: 14837) from Local Climatological Data (LCD) (National Centers for Environmental Information *et al* 2005), and removed the sites with abnormally high or low records due to potential errors of unit and calibration. As a result, observations collected from 140 sites were considered in the analysis.

Both temperature and moisture have considerable diurnal and seasonal variations, being largely influenced by the local effect and regional meteorological conditions. To best capture the localized effect on moisture and ambient temperature variability as a result of the land-atmosphere interaction, clear days with a calm or light breeze (wind speed at 10 m lower than 7 mph or 3.13 ms^{-1}) are used. We stratified the weather conditions based on the cloud coverage, precipitation, and wind speed from the aforementioned airport weather station, resulting in 156 days used in the analysis. LTER observations were aggregated from quarter-hourly to hourly. As the vegetation phenology controls evapotranspiration, directly modifying the near-surface moisture and temperature during the growing season, the data were further simplified by estimating multi-year monthly average. The local sunrise and sunset times are used to identify the hours for sub-daily estimations (day and night). The temperature threshold for EHEs is determined at the 99% quantile of daily maximum temperature from the same reference weather station during 1988–2017. Seven clear and calm EHEs were identified during the studied period.

2.2. Site environment

The footprint of observations depends on the surface roughness and the stability of the surface layer (Hsieh *et al* 2000, Schmid 2002, Allen 2006). For the selected clear and calm weather conditions, a 45 m radius buffer of each site is used to characterize the site environments according to Hsieh *et al* (2000)'s analytical model. The estimated surface characteristics of each site include the impervious surface area fraction, tree coverage fraction, and dominant land cover types from the land cover maps of the 2011 National Land Cover Database at 30 m spatial resolution (Yang *et al* 2018). The green area fraction (GAF) is estimated as the non-impervious land surface fraction for this region. The nearest distance to any water bodies (DTW) from each site is calculated in a GIS system to quantify the influence of bluespace.

2.3. Moisture and human thermal comfort

Here, we considered the absolute humidity to describe the interactive influence of green and blue spaces on moisture, which measures the actual mass of water vapor in a unit volume of dry air and best describes the total amount of moisture in the atmosphere (equation (1)). Water vapor pressure, *e* [hPa] (equation (2)) and *RH* are also used for supporting analysis as well as estimation of human comfort index —Apparent Temperature (*AT*).

$$\rho_v = \frac{216.5\, \boldsymbol{e}}{\boldsymbol{T_a} + 273.16} \tag{1}$$

$$\boldsymbol{e} = \frac{\boldsymbol{RH}^{*}\boldsymbol{e_s}}{100} \tag{2}$$

$$\boldsymbol{e_s} = 6.105\, \boldsymbol{e}^{\frac{17.27\boldsymbol{T}}{\boldsymbol{T}+237.7}} \tag{3}$$

where T_a is ambient air temperature in °C and e_s [hPa] is the saturated water vapor pressure from the Clausius-Clapeyron equation.

We used a generalized version of Steadman *AT* to measure the outdoor thermal comfort under shaded condition (Steadman 1994), including the effects of temperature, humidity, and wind speed (equation (4)). This index is designed to quantify the potential health effects of meteorological conditions and is suitable for both cold and hot temperature regimes. *AT* is currently used by the Bureau of Meteorology of Australia.

$$\mathbf{AT} = \mathbf{T_a} + 0.33\mathbf{e} - 0.70\mathbf{v_{10}} - 4.00 \tag{4}$$

where *AT* is in °C and $\boldsymbol{v_{10}}$ is the wind speed measurements at 10 m obtained from the local weather station. The spatial variation of wind speed is not considered.

2.4. Statistical modeling

We used the generalized additive models (GAMs) in the *mgcv* package of R to assess the nonlinear influence of blue and green spaces on the spatial anomaly of air temperature, absolute humidity, and *AT* on the sub-daily, daily, and monthly scale. GAMs are flexible and robust to fit multiple covariates with the nonlinear relationship by smoothing splines (Wood 2006). The response variables (e.g., T_a, and *AT*) follow the Gaussian distribution. Each predicting variable, *GAF* or *DTW*, uses the thin plate regression splines for model fitting (Wood 2006). In addition to quantifying the main effect of both greenspace and bluespace on the urban microclimate, the tensor product interaction (*ti*) between both *GAF* and *DTW* is introduced to account for their marginal interactive effect (Wood 2006). Equation (5) shows the general model structure. Model fitting was determined by the fast restricted maximum likelihood (REML) method (Wood 2011).

$$y_i = \alpha + f_1(GAF) + f_2(DTW) + f_3(GAF,\ DTW) + \epsilon_i \quad (5)$$

where y_i is the spatial anomalies of monthly temperature, absolute humidity, or apparent temperature; α is the intercept; $f_{1,2}$ are the functions of smooth terms, and f_3 is the function used to account for tensor product interaction (*ti*); ϵ is the residual error.

3. Results

3.1. Spatial anomaly of temperature and moisture

Similar to other cities, Madison is largely influenced by the local effect of urbanization and surface heterogeneity (Li *et al* 2019), where a remarkable intraurban spatial variability of temperature and absolute humidity are observed with a strong seasonality (e.g., figure 1 for July and figure S3 is available online at stacks.iop.org/ERL/15/034041/mmedia for January). The urban areas are persistently warmer than the rural areas (e.g., forest) throughout the year (figure S2). Although the urban center is located near the lakes, the atmospheric moisture level during the warm seasons at the daily scale is lower than the less urbanized areas. Diurnally, the contrast of urban moisture spatial anomaly is distinguishable by a strong daytime urban moisture deficit (UMD, figures 1(D) and S2) (Hao and Huang 2018) and a discernible nighttime urban moisture excess (UME) that is ubiquitous during the summer months (figures 1(D), S3D and S2). UMD increases with the ambient temperature, largely due to the lack of localized surface moisture sources over dominantly impervious surfaces. The nighttime UME is mainly attributable to anthropogenic moisture emission (Salmon 2018) from industry and transportation concentrated over high-density urban areas. The strong summer nighttime UHI (figure S2) reinforces UME by facilitating continuous evaporation and reducing the condensation (Holmer and Eliasson 1999).

3.2. Combined effects of greenspace and bluespace

Given the existing urban setting, we then assessed the mixed effects of greenspace and bluespace on the spatial variability of temperature, moisture, as well as their interplay measured by *AT*, which is quantified by a series of generalized additive models.

Regarding greenspace, cooling effects have been extensively documented as isolated cases at small scales, and findings broadly agree on its effectiveness for temperature reduction (Bowler *et al* 2010, Cohen *et al* 2012). How the local scale observations can be extrapolated to make conclusions at the city scale remains unclear as human activities, man-made surfaces, and water bodies co-influence the urban thermal environment. Our results show persistent diurnal and seasonal cooling in figure 2, agreeing with other local observational cases (Bowler *et al* 2010, Cohen *et al* 2012). Daytime cooling is discernible but lacks seasonality (0.8 °C ± 0.2 °C, mean ± 1 standard deviation), and the summer capacity is consistent with the other tree cooling study in the same city by 1 °C (Ziter *et al* 2019). Yet, we found that nighttime greenspace cooling is substantially greater than its daytime effect with a strong seasonality (2.4 °C ± 0.7 °C). Despite more daytime cooling via transpiration occurring during warm seasons, a stronger temperature reduction effect at night is likely attributable to the significant reduction of heat storage over places with a greater green area fraction (GAF, within a 45 m radius of each site). The nonlinearity of the greenspace cooling is observed in the summer, e.g., July-September (figures 3(A) and S4), suggesting an accelerated cooling efficiency as vegetation increasingly dominates the area (GAF greater than 50%). However, an inefficient daytime cooling in areas with less or no vegetation (GAF $<$ 50%) during the hottest months (e.g., July and August) is observed in figures 3(A) and S4 for all months.

Regarding bluespace, its temperature mitigation capacity remains inconclusive due to sparse case studies in the literature (Völker *et al* 2013). Our spatially dense observations suggest a weak daytime cooling but prominent nighttime warming on the waterside (figures 3(B), and S6 for all months). Micro-scale thermal recirculation initiated by the strong differential surface temperatures between water surfaces and adjacent land can bring cooler air inland (e.g., Murakawa *et al* 1991). However, its effect is capped to a small range of 0.2 °C–0.7 °C, mainly in spring and fall with annual average cooling of 0.2° ± 0.4 °C. Meanwhile, the daytime distance effect reaches up to approximate 0.5 km from the coastline (e.g., figure S6 for April, May, and September). The high heat capacity and heat admittance facilitate bluespaces to act as effective heat storage bodies (Heusinkveld *et al* 2014), significantly warming the waterside at night by 1.1° ± 0.6 °C on annual average (figure 2). Summer and fall show a stronger warming up to 2.3 °C, and can extend the effect up to 1 km from the shoreline. Thus, in this study, water bodies dispersed within the city center exacerbate the existing large heat storage in the densely built area at night, leading to a relatively higher temperature.

Urban thermal comfort is both spatially and temporally variable, with asymmetric diurnal dynamics due to the joint modulation by greenspace and bluespace (figure 4(C)). Evaporative cooling from greenspace and bluespace raises the ambient moisture, potentially increasing the thermal discomfort diurnally (figure 4(B)). For example, nearshore humidification and evapotranspiration compromise the bluespace and greenspace cooling to various degrees during the day. The thermal discomfort affected by higher temperatures of inland urban areas is alleviated to a certain extent by their lower humidity. On average, such trade-offs slightly reduce the annual daytime thermal spatial variation from 1.6° ± 0.4 °C to

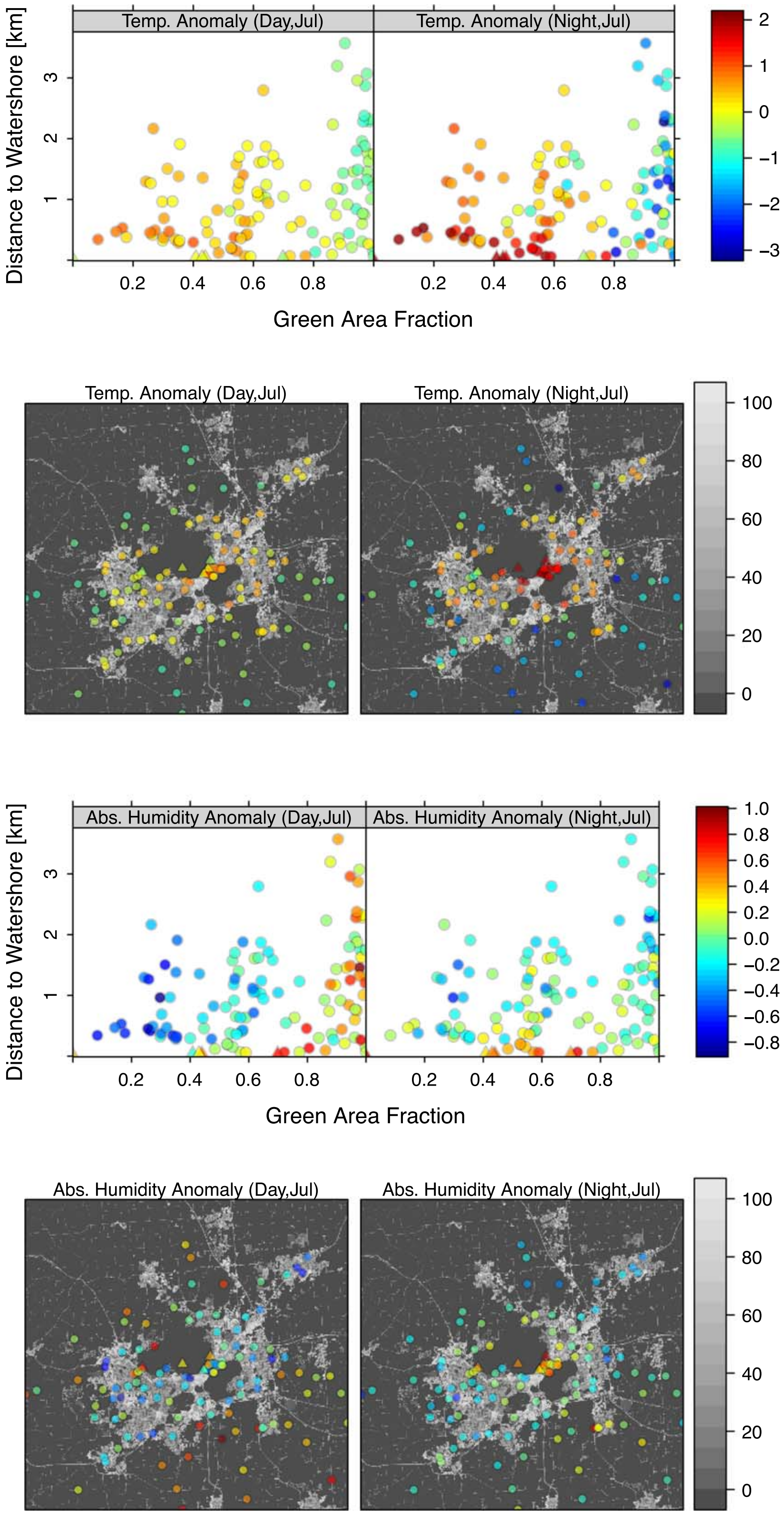

Figure 1. Spatial anomaly of air temperature [°C] (A and B) and absolute humidity [gm^{-3}] (C and D) for day and night of July, respectively. A and C show the temperature and moisture changes as a function of green area fraction (GAF) and the distance to the water shore (DTW). The color bars represent the spatial anomaly of temperature (A) and absolute humidity (C), where red is for positive anomaly and blue for a negative anomaly. Each dot indicates one site, and the triangle symbol denotes the site with nonzero water fraction within the 45 m buffer. B and D are the spatial distribution of these anomalies, and their color scheme is the same as the corresponding scatter plot. The impervious surface fraction in 30 m from the 2011 National Land Cover Database is indicated by the background in grayscale (lighter color has higher impervious surface fraction).

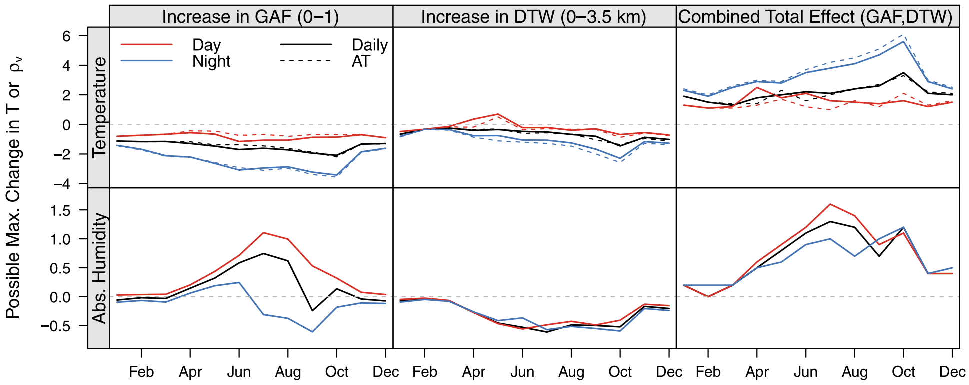

Figure 2. The annual cycle of maximum change in ambient temperature and absolute humidity as a function of green area fraction (GAF) or the distance away from the water shore (DTW), and their combined maximum effect on thermal regulation. The main effects of GAF and DTW are the summary of results from figure S4–S9 in the Supplementary Materials. The sign of changes is determined by the trend as an increase in GAF or DTW from GAF = 0 and DTW = 0 km. The absolute magnitude of maximum changes as a result of interaction between GAF and DTW is shown in the third column, which is summarized from the Generalized Additive Models (GAM) in figure S10–S15. The dashed line and shaded area indicate the change in apparent temperature (AT) and the difference between T and AT, respectively.

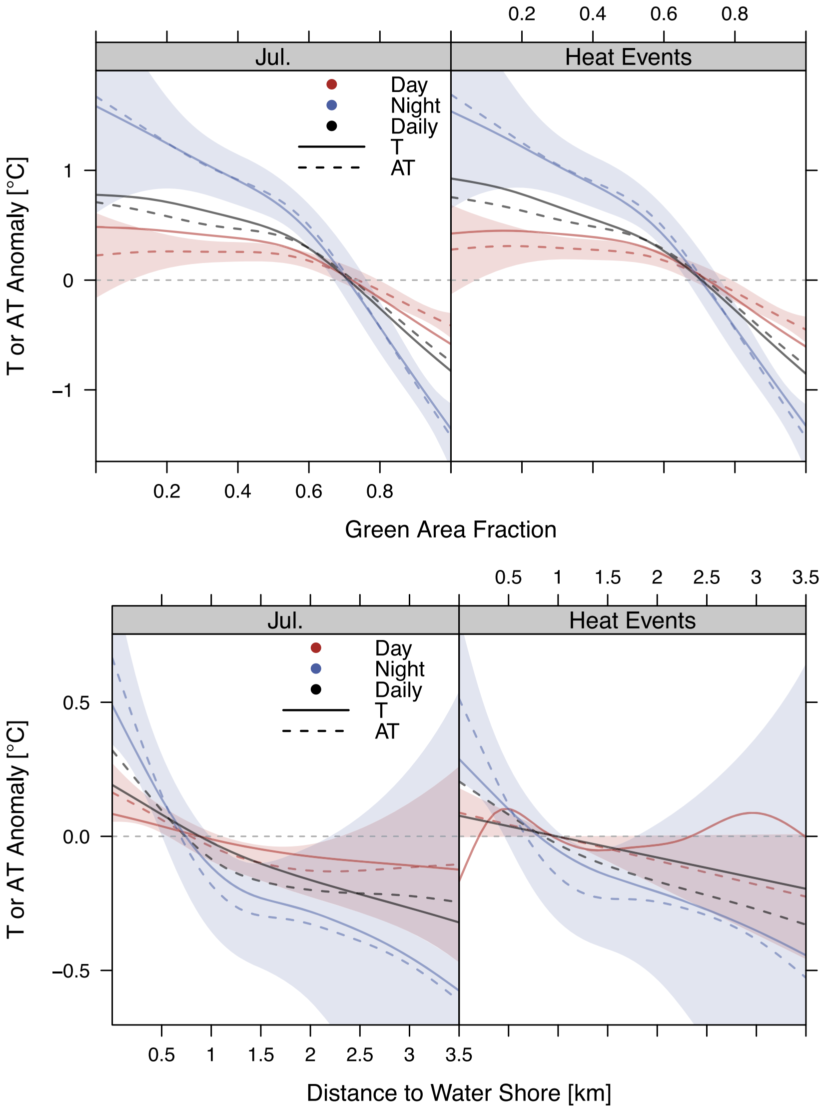

Figure 3. The main effect of green and blue spaces on temperature (T) and apparent temperature (AT) for normal Jul. and extreme hot days, respectively. The dashed lines are for AT and solid lines represent T. The shaded region indicates the 2 standard errors of AT (dashed line).

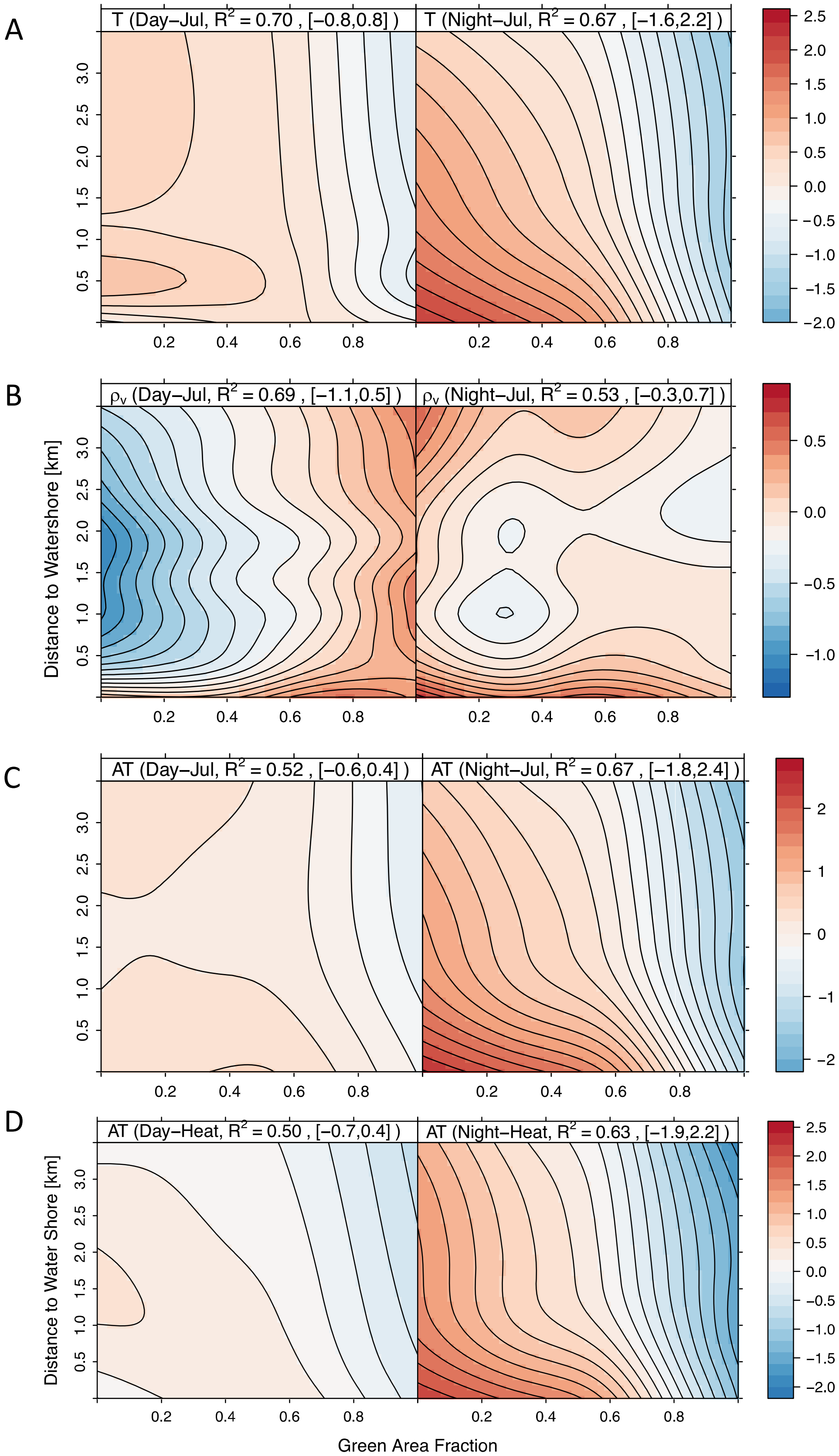

Figure 4. Estimations of combined effect of green area fraction and the distance to the water shore on the ambient air temperature, absolute humidity, and the apparent temperature for day (left column) and night (right column) in Jul. and during the extreme hot events. The coefficient of determination (R^2) of GAMs and the estimated range for spatial anomaly are labeled in the parentheses.

$1.4° \pm 0.3$ °C. On the other hand, high ambient humidity may reduce the daytime efficiency of evaporative and transpiration cooling by blue and green spaces. As a result, the daytime local ambient temperature hotspot shifts from the high-density lakeshore urban areas to nearshore mid-density urban areas during the spring and summer months (figures 4(A) and (C) for July and figure S14 for all months). At night, bluespace humidification intensifies the summer discomfort near the lake, while the prevalence of the nighttime UME (figure S13) during July-September reinforces the strong UHI, both of which synergistically enhance the discomfort of nearshore urban areas by 4.2 °C in July with a maximum effect of 6.1 °C in October. In contrast, highly vegetated areas have lower nighttime temperatures and are less prone to warming by proximity to water bodies (figures 4(C) and S15). Moreover, we observe strong interactions between green and blue spaces for GAF less than 0.6 and DTW within 1.5 km at night, while for GAF greater than 0.6, the cooling capacity of greenspace is barely affected by the bluespaces (figure 4(A)).

The comparison of the asymmetric joint effects of greenspace and bluespace at diurnal and seasonal scales suggests that more effective nighttime cooling occurs during warm seasons (figure 2). Greenspace plays an equal or more influential role in thermal environment modulation (figure 2) as a result of the strong control from the local land cover. The annual mean daytime effect on thermal change by the combination of green and blue spaces is $1.4° \pm 0.3$ °C on annual average, where the independent respective contributions are $0.7° \pm 0.1$ °C for greenspace and $0.4° \pm 0.2$ °C for bluespace. Such collective effects create a large spatial variability of nighttime thermal discomfort ($3.5° \pm 1.2$ °C), which exceeds daytime spatial variability by 1.6 to 4.3 times depending on the season. At the annual scale, we observed spatial variability of $2.5° \pm 0.7$ °C contributed from greenspace and $1.2° \pm 0.6$ °C contributed from bluespace. The stronger benefit achieved by greenspace cooling can be up to $3.0° \pm 0.5$ °C during warm nights (e.g., April-October). However, no significant seasonal variation of daytime thermal regulation was observed.

3.3. Cooling capacity changes during extreme heat events

The daily mean temperature during the studied EHEs is about 3.3 °C warmer than that in July. The greenspace still played a dominant role in air temperature modulation during EHEs (figure 3(A)). However, we observed an enhanced daytime cooling effect of bluespace by up to 0.3 °C during the EHEs compared to warming up to 0.2 °C in July (table 1 and figure 3(B)). The regional moisture was also increased with an enhanced spatial variability (figure S1(A) and B). The daytime excess moisture dampened the cooling from greenspace and bluespace during extreme heat days, resulting in an unchanged overall thermal mitigation effect of 1.1 °C compared to July (table 1). During EHEs, the hotspot of heat exposure shifts from the nearshore, mid-density urban areas on normal July days to high-density urban areas at some distance (about 1.5 km) from the shore (figures 4(C) and (D)). The hotspot shift can be important even though the range of temperature variation is small, given the overall high thermal discomfort at 33.1 °C. The synergistic bluespace warming from temperature and moisture slightly decreased during the hottest nights. Similar to daytime, the thermal comfort regulation capacity of green and blue spaces showed negligible changes at night (up to 4.1 °C for extreme events versus 4.2 °C for normal nights in July) (table 1). Overall thermal discomfort was exacerbated by 4.5 °C during the extreme events. The nearshore downtown residents were likely to be exposed to up to 8.6 °C of excess heat as a result of synoptic weather conditions and local urbanization effects. In summary, bluespace exhibits an enhanced ambient temperature reduction benefit during extremely hot days, but its effects are offset by elevated humidity.

4. Discussion and conclusions

Water bodies located within or near urban areas are a common landscape feature in many cities worldwide. However, given the presence of natural water bodies in urban areas, what is the expected cooling effect of existing or additional urban greenspace? New insight into the non-trivial interactive influences of green and blue spaces can provide an improved understanding and offer flexible options to reduce urban residents' exposure to heat risks. The potentially hazardous health impacts of nighttime heat stress are augmented in the summer months by bluespace warming, especially if the near-shore areas are characterized by dense urban developments (Theeuwes *et al* 2013, Steeneveld *et al* 2014, Targino *et al* 2019). Keeping a certain distance away from water bodies (>0.5 km) and/or increasing greenspace to a considerable level (>0.6 *GAF*) are both viable long-term solutions to reduce nighttime heat exposure of vulnerable population groups during the hottest months or during heat events.

The daytime synergistic cooling from both green and blue spaces are discernible but less significant compared to the strong nighttime cooling of greenspace regardless of the season. In Madison WI, a temperate climate city, we found clear day-night asymmetry in temperature modulation effectiveness under both normal and extreme conditions, suggesting that additional heat reduction approaches should be considered to offset the hottest hours of summer days as well as EHEs. Furthermore, greenspace is still more efficient for daytime temperature reduction in contrast to the bluespace, which is consistent with a

Table 1. Summary of individual and combined cooling effect of green and blue spaces in Jul. and extreme heat events. $\bar{T}$ and $\overline{AT}$ represent the spatial mean of air temperature and apparent temperature during the selected period. ΔC describes the maximum thermal regulation capacity as a combined effect of green and blue spaces, which is an absolute magnitude and always positive. ΔGAF and ΔDTW shows the maximum cooling (negative) or warming (positive) of greenspace (GAF) and bluespace (DTW) respectively.

Mean (Δ)	Daily [°C]		Day [°C]		Night [°C]	
	Heat	Jul.	Heat	Jul.	Heat	Jul.
$\bar{T}(T_{\Delta C})$	29.2 (3.3)	25.9 (2.1)	31.2 (2.1)	27.6 (1.6)	25.7 (3.3)	22.3 (3.8)
$\overline{AT}$ $(AT_{\Delta C})$	31.6 (1.9)	27.3 (2.0)	33.1 (1.1)	28.7 (1.0)	28.8 (4.1)	24.3 (4.2)
$(T_{\Delta GAF}, \text{-} T_{\Delta DTW})$	(−1.8, 0.3)	(−1.6, 0.5)	(−1.1, −0.3)	(−1.1, 0.2)	(−2.9, 0.7)	(−2.9, 1.1)
$(AT_{\Delta GAF}, \text{-} AT_{\Delta DTW})$	(−1.5, 0.5)	(−1.5, 0.6)	(−0.8, 0.3)	(−0.7, 0.3)	(−3.1, 1.0)	(−3.1, 1.3)

recent short-term observational study over a mid-size Brazilian city in the tropical climate (Targino *et al* 2019). Moreover, shade from urban trees can immediately reduce the radiation heat load and alleviate the perceived heat stress, although that effect is not explicitly assessed in this study. The daytime cooling of bluespace varies seasonally in our study with a maximum of 0.7 °C in May and it can be enhanced during EHEs, while the increased moisture counteracts the temperature cooling and makes the overall influence less significant. The different impacts of blue and green spaces on urban microclimate suggest that greenspace has a more predictable control on thermal regulation.

There are two main caveats to this study. First, effects of anthropogenic heat and moisture (e.g. from traffic emissions, building energy use, industrial processes and human metabolism) are not addressed and may co-vary with *GAF* or *DTW*. Since anthropogenic heat and moisture emission tends to be the most intense in highly developed urban areas, the actual cooling rate of greenspace can be slightly overestimated. However, anthropogenic heat flux contributes less significantly to the surface energy budget than the storage heat flux for a mid-size city (Oke *et al* 2017). Second, the effects of greenspace and bluespace are measured differently. We consider a fixed buffer size (45 m radius) to account for the main signal of greenspace cooling. However, there is a spillover effect of greenspace cooling on the surrounding area, but it is much weaker than the effect of bluespace (ranging from a few meters up to 100 m) (Aram *et al* 2019, Ziter *et al* 2019). The cooling effect can vary slightly for different footprint sizes (Ziter *et al* 2019). We have assessed the effect of footprint size on the greenspace cooling at 30 m and 60 m compared to the 45 m buffer radius (see figure S18). The diurnal and seasonal cooling trends remain the same but a decreasing cooling magnitude is found as the buffer size increases. The scale effect is more sensitive at night with an annual average of 0.2 °C while the daytime variation is negligible at about 0.02 °C.

The elevated thermal discomfort and increased excess heat exposure during the extremely hot days in the urban areas raise a public health concern. We holistically assessed the effectiveness of green and blue spaces and their interactive influence on the urban thermal environment for heat mitigation, and provided recommendations for long-term urban heat mitigation. The nighttime bluespace warming and humidification exacerbate the existing urban thermal discomfort at the dense urban core close to the shore by 4.2 °C in the hottest month with annual average warming by 3.5 ± 1.2 °C. This magnitude can be influential as strong evidence has been established between hot nighttime temperatures and mortality (Murage *et al* 2017). We show for the first time that, remarkably, the degree of bluespace warming depends upon the amount of vegetation at the city scale. Greenspace has a stronger cooling capacity than bluespace, and its thermal modulation capacity does not show a significant change during EHEs. These findings and underlying mechanisms will be examined across multiple cities in future studies. Our method is transferable to other cities with a spatially-dense observational network or spatiotemporal data from various emerging techniques, such as mobile sensing with manned or unmanned vehicles, and crowd-sourced citizen science, that could be used to support the sustainable development of multi-scale and interdependent urban systems.

Acknowledgments

The authors would like to thank Drs Ying Sun, Linda Shi, and Wilfried Brutsaert, and Zhihua Wang for their constructive comments on the manuscript, and the Cornell Statistics Consulting Unit, Drs Yang Ning and Sumanta Basu for their help on statistical models. The authors also aknowlege the critial review by two anonymous reviewers on an earlier version of this manuscript. Particular thanks to NSF-funded Long-Term Ecological Research of North Temperate Lakes site for free data (PI: Christopher Kucharik). This work was supported in part by internal initiation grants from the University of Alabama in Huntsville and Cornell University.

Data availability statement

The data that support the findings of this study are available from the corresponding author upon reasonable request. The original datasets are publicly available from https://lter.limnology.wisc.edu/content/wsc-temperature-and-relative-humidity-data-150-locations-and-around-madison-wisconsin-2012.

ORCID iDs

Leiqiu Hu https://orcid.org/0000-0002-1867-2521
Qi Li https://orcid.org/0000-0003-4435-6220

References

Adelia A S, Yuan C, Liu L and Shan R Q 2019 Effects of urban morphology on anthropogenic heat dispersion in tropical high-density residential areas *Energy Build.* **186** 368–83

Allen R G 2006 Footprint analysis to assess the conditioning of temperature and humidity measurements *a Weather Station Vicinity World Environmental and Water Resource Congress 2006* (Reston, VA: American Society of Civil Engineers) pp 1–12

Aram F, Higueras García E, Solgi E and Mansournia S 2019 Urban green space cooling effect in cities *Heliyon* **5** e01339

Bowler D E, Buyung-Ali L, Knight T M and Pullin A S 2010 Urban greening to cool towns and cities: a systematic review of the empirical evidence *Landsc. Urban Plan.* **97** 147–55

Cohen P, Potchter O and Matzarakis A 2012 Daily and seasonal climatic conditions of green urban open spaces in the Mediterranean climate and their impact on human comfort *Build. Environ.* **51** 285–95

Coutts A, Loughnan M, Tapper N, White E, Thom J, Broadbent A and Harris R 2014 *Impacts of water sensitive urban design solutions on human thermal comfort* Online (http://watersensitivecities.org.au/wp-content/uploads/2015/01/GreenCitiesandMicroclimate-no2.pdf)

Frantzeskaki N *et al* 2019 Nature-based solutions for Urban climate change adaptation: linking science, policy, and practice communities for evidence-based decision-making *Bioscience* **69** 455–66

Grimm N B, Faeth S H, Golubiewski N E, Redman C L, Wu J, Bai X and Briggs J M 2008 Global change and the ecology of cities *Science (80-.).* **319** 756–60

Grimmond S 2007 Urbanization and global environmental change: local effects of urban warming *Geogr. J.* **173** 83–8

Gunawardena K R, Wells M J and Kershaw T 2017 Utilising green and bluespace to mitigate urban heat island intensity *Sci. Total Environ.* **584–585** 1040–55

Guo Y *et al* 2018 Quantifying excess deaths related to heatwaves under climate change scenarios: a multicountry time series modelling study ed J A Patz PLOS*Med.* **15** e1002629

Hao L and Huang X 2018 Ecohydrological processes explain Urban Dry Island effects in a wet region *Southern China* 1–15

He B-J, Ding L and Prasad D 2019a Enhancing urban ventilation performance through the development of precinct ventilation zones: a case study based on the Greater Sydney *Australia Sustain. Cities Soc.* **47** 101472

He B-J, Zhu J, Zhao D-X, Gou Z-H, Qi J-D and Wang J 2019b Co-benefits approach: opportunities for implementing sponge city and urban heat island mitigation *Land use Policy* **86** 147–57

Heusinkveld B G, Steeneveld G J, Van Hove L W A, Jacobs C M J and Holtslag A A M 2014 Spatial variability of the rotterdam urban heat island as influenced by urban land use *J. Geophys. Res.* **119** 677–92

Holmer B and Eliasson I 1999 Urban-rural vapour pressure differences and their role in the development of urban heat islands *Int. J. Climatol.* **19** 989–1009

Hsieh C-I, Katul G and Chi T 2000 An approximate analytical model for footprint estimation of scalar fluxes in thermally stratified atmospheric flows *Adv. Water Resour.* **23** 765–72

Hu L, Monaghan A J and Brunsell N A 2015 Investigation of Urban Air Temperature and Humidity Patterns during Extreme Heat Conditions Using Satellite-Derived Data *J. Appl. Meteorol. Climatol.* **54** 2245–59

Kapsalis V C, Vardoulakis E and Karamanis D 2014 Simulation of the cooling effect of the roof-added photovoltaic panels *Adv. Build. Energy Res.* **8** 41–54

Kucharik C 2018 WSC—Temperature and relative humidity data from 150 locations in and around Madison, Wisconsin from 2012–2017 (https://lter.limnology.wisc.edu/content/wsc-temperature-and-relative-humidity-data-150-locations-and-around-madison-wisconsin-2012)

Li D, Liao W, Rigden A J, Liu X, Wang D, Malyshev S and Shevliakova E 2019 Urban heat island: aerodynamics or imperviousness? *Sci. Adv.* **5** eaau4299

Ma S, Goldstein M, Pitman A J, Haghdadi N and MacGill I 2017 Pricing the urban cooling benefits of solar panel deployment in Sydney *Australia Sci. Rep.* **7** 43938

Murage P, Hajat S and Kovats R S 2017 Effect of night-time temperatures on cause and age-specific mortality in London *Environ. Epidemiol.* 1

Murakawa S, Sekine T, Narita K and Nishina D 1991 Study of the effects of a river on the thermal environment in an urban area *Energy Build.* **16** 993–1001

National Centers for Environmental Information, NESDIS, NOAA U S D of C, National Weather Service, NOAA U S D of C, U.S. Air Force U S D of D and Federal Aviation Agency U S D of T 2005 US Local Climatological Data (LCD) Online (https://data.nodc.noaa.gov/cgi-bin/iso?id=gov.noaa.ncdc:C00684#)

Oke T 1995 The heat island of the urban boundary layer: characteristics, causes and effects *Wind Clim. Cities* 81–107

Oke T R 1988 Street design and urban canopy layer climate *Energy Build.* **11** 103–13

Oke T R, Crowther J M, McNaughton K G, Monteith J L and Gardiner B 1989 The Micrometeorology of the Urban Forest [and Discussion] *Philos. Trans. R. Soc. B Biol. Sci.* **324** 335–49

Oke T R, Mills G, Christen A and Voogt J A 2017 *Urban Climates* (Cambridge: Cambridge University Press)

Oleson K W, Monaghan A, Wilhelmi O, Barlage M, Brunsell N, Feddema J, Hu L and Steinhoff D F 2015 Interactions between urbanization, heat stress, and climate change *Clim. Change* **129** 525–41

Rahman M A, Armson D and Ennos A R 2015 A comparison of the growth and cooling effectiveness of five commonly planted urban tree species *Urban Ecosyst.* **18** 371–89

Rahmstorf S and Coumou D 2011 Increase of extreme events in a warming world *Proc. Natl Acad. Sci. USA* **108** 17905–9

Salmon O E 2018 Urban atmospheric water vapor and its stable isotopologues *Dissertation* Purdue University

Santamouris M, Ding L, Fiorito F, Oldfield P, Osmond P, Paolini R, Prasad D and Synnefa A 2017 Passive and active cooling for the outdoor built environment—Analysis and assessment of the cooling potential of mitigation technologies using performance data from 220 large scale projects *Sol. Energy* **154** 14–33

Schatz J and Kucharik C J 2014 Seasonality of the urban heat island effect in Madison, Wisconsin *J. Appl. Meteorol. Climatol.* **53** 2371–86

Schmid H P 2002 Footprint modeling for vegetation atmosphere exchange studies: a review and perspective *Agric. For. Meteorol.* **113** 159–83

Seneviratne S I, Phipps S J, Pitman A J, Hirsch A L, Davin E L, Donat M G, Hirschi M, Lenton A, Wilhelm M and Kravitz B 2018 Land radiative management as contributor to regional-scale climate adaptation and mitigation *Nat. Geosci.* **11** 88–96

Small C 2004 Global population distribution and urban land use in geophysical parameter space *Earth Interact.* **8** 1–18

Steadman R G 1994 Norms of apparent temperature in Australia *Aust. Meteorol. Mag.* **43** 1–16

Steeneveld G J, Koopmans S, Heusinkveld B G and Theeuwes N E 2014 Refreshing the role of open water surfaces on mitigating the maximum urban heat island effect *Landsc. Urban Plan.* **121** 92–6

Steffen W *et al* 2018 Trajectories of the Earth System in the Anthropocene *Proc. Natl Acad. Sci.* **115** 8252–9

Targino A C, Coraiola G C and Krecl P 2019 Green or blue spaces? Assessment of the effectiveness and costs to mitigate the urban heat island in a Latin American city *Theor. Appl. Climatol.* **136** 971–84

Theeuwes N E, Solcerová A and Steeneveld G J 2013 Modeling the influence of open water surfaces on the summertime temperature and thermal comfort in the city *J. Geophys. Res. Atmos.* **118** 8881–96

US Census Bureau/Population Division 2019 *Annual Estimates of the Resident Population: April 1, 2010 to July 1, 2018*

Völker S, Baumeister H, Classen T, Hornberg C and Kistemann T 2013 Evidence for the temperature-mitigating capacity of urban blue space - A health geographic perspective *Erdkunde* **67** 355–71

Wood S N 2011 Fast stable restricted maximum likelihood and marginal likelihood estimation of semiparametric generalized linear models *J. R. Stat. Soc. Ser. B (Statistical Methodol.* **73** 3–36

Wood S N 2006 Low-rank scale-invariant tensor product smooths for generalized additive mixed models *Biometrics* **62** 1025–36

Yang L *et al* 2018 NLCD 2011 Land Cover (CONUS) *Multi-Resolution L. Charact. Cionsortium* Online: (https://mrlc.gov/data/nlcd-2011-land-cover-conus-0)

Ziter C D, Pedersen E J, Kucharik C J and Turner M G 2019 Scale-dependent interactions between tree canopy cover and impervious surfaces reduce daytime urban heat during summer *Proc. Natl Acad. Sci.* **116** 7575–80